# *Planck* 2015 results. XI. CMB power spectra, likelihoods, and robustness of parameters

Planck Collaboration: N. Aghanim[63], M. Arnaud[78], M. Ashdown[74,6], J. Aumont[63], C. Baccigalupi[91], A. J. Banday[103,10], R. B. Barreiro[69],
J. G. Bartlett[1,71], N. Bartolo[32,70], E. Battaner[105,106], K. Benabed[64,102], A. Benoît[61], A. Benoit-Lévy[24,64,102], J.-P. Bernard[103,10], M. Bersanelli[35,51],
P. Bielewicz[86,10,91], J. J. Bock[71,12], A. Bonaldi[72], L. Bonavera[20], J. R. Bond[9], J. Borrill[15,96], F. R. Bouchet[64,94*], F. Boulanger[63], M. Bucher[1],
C. Burigana[50,33,52], R. C. Butler[50], E. Calabrese[98], J.-F. Cardoso[79,1,64], A. Catalano[80,77], A. Challinor[66,74,13], H. C. Chiang[28,7], P. R. Christensen[87,38],
D. L. Clements[59], L. P. L. Colombo[23,71], C. Combet[80], A. Coulais[77], B. P. Crill[71,12], A. Curto[69,6,74], F. Cuttaia[50], L. Danese[91], R. D. Davies[72],
R. J. Davis[72], P. de Bernardis[34], A. de Rosa[50], G. de Zotti[47,91], J. Delabrouille[1], F.-X. Désert[57], E. Di Valentino[64,94], C. Dickinson[72], J. M. Diego[69],
K. Dolag[104,84], H. Dole[63,62], S. Donzelli[51], O. Doré[71,12], M. Douspis[63], A. Ducout[64,59], J. Dunkley[98], X. Dupac[40], G. Efstathiou[74,66],
F. Elsner[24,64,102], T. A. Enßlin[84], H. K. Eriksen[67], J. Fergusson[13], F. Finelli[50,52], O. Forni[103,10], M. Frailis[49], A. A. Fraisse[28], E. Franceschi[50],
A. Frejsel[87], S. Galeotta[49], S. Galli[73], K. Ganga[1], C. Gauthier[1,83], M. Gerbino[100,89,34], M. Giard[103,10], E. Gjerløw[67], J. González-Nuevo[20,69],
K. M. Górski[71,107], S. Gratton[74,66], A. Gregorio[36,49,56], A. Gruppuso[50,52], J. E. Gudmundsson[100,89,28], J. Hamann[101,99], F. K. Hansen[67],
D. L. Harrison[66,74], S. Henrot-Versillé[76], C. Hernández-Monteagudo[14,84], D. Herranz[69], S. R. Hildebrandt[71,12], E. Hivon[64,102],
W. A. Holmes[71], A. Hornstrup[17], K. M. Huffenberger[26], G. Hurier[63], A. H. Jaffe[59], W. C. Jones[28], M. Juvela[27], E. Keihänen[27], R. Keskitalo[15],
K. Kiiveri[27,45], J. Knoche[84], L. Knox[29], M. Kunz[18,63,3], H. Kurki-Suonio[27,45], G. Lagache[5,63], A. Lähteenmäki[2,45], J.-M. Lamarre[77], A. Lasenby[6,74],
M. Lattanzi[33,53], C. R. Lawrence[71], M. Le Jeune[1], R. Leonardi[8], J. Lesgourgues[65,101], F. Levrier[77], A. Lewis[25], M. Liguori[32,70], P. B. Lilje[67],
M. Lilley[64,94], M. Linden-Vørnle[17], V. Lindholm[27,45], M. López-Caniego[40], J. F. Macías-Pérez[80], B. Maffei[72], G. Maggio[49], D. Maino[35,51],
N. Mandolesi[50,33], A. Mangilli[63,76], M. Maris[49], P. G. Martin[9], E. Martínez-González[69], S. Masi[34], S. Matarrese[32,70,42], P. R. Meinhold[30],
A. Melchiorri[34,54], M. Migliaccio[66,74], M. Millea[29], S. Mitra[58,71], M.-A. Miville-Deschênes[63,9], A. Moneti[64], L. Montier[103,10], G. Morgante[50],
D. Mortlock[59], S. Mottet[64,94], D. Munshi[93], J. A. Murphy[85], A. Narimani[22], P. Naselsky[88,39], F. Nati[28], P. Natoli[33,4,53], F. Noviello[72], D. Novikov[82],
I. Novikov[87,82], C. A. Oxborrow[17], F. Paci[91], L. Pagano[34,54], F. Pajot[63], D. Paoletti[50,52], B. Partridge[44], F. Pasian[49], G. Patanchon[1], T. J. Pearson[12,60],
O. Perdereau[76], L. Perotto[80], V. Pettorino[43], F. Piacentini[34], M. Piat[1], E. Pierpaoli[23], D. Pietrobon[71], S. Plaszczynski[76], E. Pointecouteau[103,10],
G. Polenta[4,48], N. Ponthieu[63,57], G. W. Pratt[78], S. Prunet[64,102], J.-L. Puget[63], J. P. Rachen[21,84], M. Reinecke[84], M. Remazeilles[72,63,1], C. Renault[80],
A. Renzi[37,55], I. Ristorcelli[103,10], G. Rocha[71,12], M. Rossetti[35,51], G. Roudier[1,77,71], B. Rouillé d'Orfeuil[76], J. A. Rubiño-Martín[68,19], B. Rusholme[60],
L. Salvati[34], M. Sandri[50], D. Santos[80], M. Savelainen[27,45], G. Savini[90], D. Scott[22], P. Serra[63], L. D. Spencer[93], M. Spinelli[76], V. Stolyarov[6,97,75],
R. Stompor[1], R. Sunyaev[84,95], D. Sutton[66,74], A.-S. Suur-Uski[27,45], J.-F. Sygnet[64], J. A. Tauber[41], L. Terenzi[92,50], L. Toffolatti[20,69,50],
M. Tomasi[35,51], M. Tristram[76], T. Trombetti[50,33], M. Tucci[18], J. Tuovinen[11], G. Umana[46], L. Valenziano[50], J. Valiviita[27,45], F. Van Tent[81],
P. Vielva[69], F. Villa[50], L. A. Wade[71], B. D. Wandelt[64,102,31], I. K. Wehus[71,67], D. Yvon[16], A. Zacchei[49], and A. Zonca[30]

*(Affiliations can be found after the references)*

Preprint online version: 1st July 2016

## Abstract

This paper presents the *Planck* 2015 likelihoods, statistical descriptions of the 2-point correlation functions of the cosmic microwave background (CMB) temperature and polarization fluctuations that account for relevant uncertainties, both instrumental and astrophysical in nature. They are based on the same hybrid approach used for the previous release, i.e., a pixel-based likelihood at low multipoles ($\ell < 30$) and a Gaussian approximation to the distribution of cross-power spectra at higher multipoles. The main improvements are the use of more and better processed data and of *Planck* polarization information, along with more detailed models of foregrounds and instrumental uncertainties. The increased redundancy brought by more than doubling the amount of data analysed enables further consistency checks and enhanced immunity to systematic effects. It also improves the constraining power of *Planck*, in particular with regard to small-scale foreground properties. Progress in the modelling of foreground emission enables the retention of a larger fraction of the sky to determine the properties of the CMB, which also contributes to the enhanced precision of the spectra. Improvements in data processing and instrumental modelling further reduce uncertainties. Extensive tests establish the robustness and accuracy of the likelihood results, from temperature alone, from polarization alone, and from their combination.
For temperature, we also perform a full likelihood analysis of realistic end-to-end simulations of the instrumental response to the sky, which were fed into the actual data processing pipeline; this does not reveal biases from residual low-level instrumental systematics. Even with the increase in precision and robustness, the ΛCDM cosmological model continues to offer a very good fit to the *Planck* data. The slope of the primordial scalar fluctuations, $n_{\rm s}$, is confirmed smaller than unity at more than $5\,\sigma$ from *Planck* alone. We further validate the robustness of the likelihood results against specific extensions to the baseline cosmology, which are particularly sensitive to data at high multipoles. For instance, the effective number of neutrino species remains compatible with the canonical value of 3.046.
For this first detailed analysis of *Planck* polarization spectra, we concentrate at high multipoles on the *E* modes, leaving the analysis of the weaker *B* modes to future work. At low multipoles we use temperature maps at all *Planck* frequencies along with a subset of polarization data. These data take advantage of *Planck*'s wide frequency coverage to improve the separation of CMB and foreground emission. Within the baseline ΛCDM cosmology this requires $\tau = 0.078 \pm 0.019$ for the reionization optical depth, which is significantly lower than estimates without the use of high-frequency data for explicit monitoring of dust emission. At high multipoles we detect residual systematic errors in *E* polarization, typically at the $\mu K^2$ level; we therefore choose to retain temperature information alone for high multipoles as the recommended baseline, in particular for testing non-minimal models. Nevertheless, the high-multipole polarization spectra from *Planck* are already good enough to enable a separate high-precision determination of the parameters of the ΛCDM model, showing consistency with those established independently from temperature information alone.

**Key words.** cosmic background radiation – cosmology: observations – cosmological parameters – methods: data analysis

# 1. Introduction

This paper presents the angular power spectra of the cosmic microwave background (CMB) and the related likelihood functions, calculated from *Planck*[1] 2015 data, which consists of intensity maps from the full mission, along with a subset of the polarization data.

The CMB power spectra contain all of the information available if the CMB is statistically isotropic and distributed as a multivariate Gaussian. For realistic data, these must be augmented with models of instrumental noise, of other instrumental systematic effects, and of contamination from astrophysical foregrounds.

The power spectra are, in turn, uniquely determined by the underlying cosmological model and its parameters. In temperature, the power spectrum has been measured over large fractions of the sky by the Cosmic Background Explorer (COBE; Wright et al. 1996) and the Wilkinson Microwave Anistropy Probe (WMAP; Bennett et al. 2013), and in smaller regions by a host of balloon- and ground-based telescopes (e.g., Netterfield et al. 1997; Hanany et al. 2000; Grainge et al. 2003; Pearson et al. 2003; Tristram et al. 2005b; Jones et al. 2006; Reichardt et al. 2009; Fowler et al. 2010; Das et al. 2011; Keisler et al. 2011; Story et al. 2012; Das et al. 2013). The *Planck* 2013 power spectrum and likelihood were discussed in Planck Collaboration XV (2014, hereafter Like13).

The distribution of temperature and polarization on the sky is further affected by gravitational lensing by the inhomogeneous mass distribution along the line of sight between the last scattering surface and the observer. This introduces correlations between large and small scales, which can be estimated by computing the expected contribution of lensing to the 4-point function (i.e., the trispectrum). This can in turn be used to determine the power spectrum of the lensing potential, as is done in Planck Collaboration XV (2016) for this *Planck* release, and to further constrain the cosmological parameters via a separate likelihood function (Planck Collaboration XIII 2016).

Over the last decade, CMB intensity (temperature) has been augmented by linear polarization data (e.g., Kovac et al. 2002; Kogut et al. 2003; Sievers et al. 2007; Dunkley et al. 2009; Pryke et al. 2009; QUIET Collaboration et al. 2012; Polarbear Collaboration et al. 2014). Because linear polarization is given by both an amplitude and direction, it can, in turn, be decomposed into two coordinate-independent quantities, each with a different dependence on the cosmology (e.g., Seljak 1997; Kamionkowski et al. 1997; Zaldarriaga & Seljak 1997). One, the so-called $E$ mode, is determined by much the same physics as the intensity, and therefore enables an independent measurement of the background cosmology, as well as a determination of some new parameters (e.g., the reionization optical depth). The other polarization observable, the $B$ mode, is only sourced at early times by gravitational radiation, as produced, for example, during an inflationary epoch. The $E$ and $B$ components are also conventionally taken to be isotropic Gaussian random fields, with only $E$ expected to be correlated with intensity. Thus we expect to be able to measure four independent power spectra,

namely the three auto-spectra $C_\ell^{TT}$, $C_\ell^{EE}$, and $C_\ell^{BB}$, along with the cross-spectrum $C_\ell^{TE}$.

Estimating these spectra from the likelihood requires cleaned and calibrated maps for all *Planck* detectors, along with a quantitative description of their noise properties. The required data processing is discussed in Planck Collaboration II (2016), Planck Collaboration III (2016), Planck Collaboration IV (2016), Planck Collaboration V (2016), and Planck Collaboration VI (2016) for the low-frequency instrument (LFI; 30, 44, and 70 GHz) and Planck Collaboration VII (2016) and Planck Collaboration VIII (2016) for the high-frequency instrument (HFI; 100, 143, 217, 353, 585, and 857 GHz). Although the CMB is brightest over 70–217 GHz, the full range of *Planck* frequencies is crucial to distinguish between the cosmological component and sources of astrophysical foreground emission, present in even the cleanest regions of sky. We therefore use measurements from those *Planck* bands dominated by such emission as a template to model the foreground in the bands where the CMB is most significant.

This paper presents the $C_\ell^{TT}$, $C_\ell^{EE}$, and $C_\ell^{TE}$ spectra, likelihood functions, and basic cosmological parameters from the *Planck* 2015 release. A complete analysis in the context of an extended $\Lambda$CDM cosmology of these and other results from *Planck* regarding the lensing power spectrum results, as well as constraints from other observations, is given in Planck Collaboration XIII (2016). Wider extensions to the set of models are discussed in other *Planck* 2015 papers; for example, Planck Collaboration XIV (2016) examines specific models for the dark energy component and extensions to general relativity, and Planck Collaboration XX (2016) discusses inflationary models.

This paper shows that the contribution of high-$\ell$ systematic errors to the polarization spectra are at quite a low level (of the order of a few $\mu K^2$), therefore enabling an interesting comparison of the polarization-based cosmological results with those derived from $C_\ell^{TT}$ alone. We therefore discuss the results for $C_\ell^{TE}$ and $C_\ell^{EE}$ at high multipoles. However, the technical difficulties involved with polarization measurements and subsequent data analysis, along with the inherently lower signal-to-noise ratio (especially for $B$ modes), thus require a careful understanding of the random noise and instrumental and astrophysical systematic effects. For this reason, at large angular scales (i.e., low multipoles $\ell$) the baseline results use only a subset of *Planck* polarization data.

Because of these different sensitivities to systematic errors at different angular scales, as well as the increasingly Gaussian behaviour of the likelihood function at smaller angular scales, we adopt a hybrid approach to the likelihood calculation (Efstathiou 2004, 2006), splitting between a direct calculation of the likelihood on large scales and the use of pseudo-spectral estimates at smaller scales, as we did for the previous release.

The plan of the paper reflects this hybrid approach along with the importance of internal tests and cross-validation. In Sect. 2, we present the low-multipole ($\ell < 30$) likelihood and its validation. At these large scales, we compute the likelihood function directly in pixel space; the temperature map is obtained by a Gibbs sampling approach in the context of a parameterized foreground model, while the polarized maps are cleaned of foregrounds by a template removal technique.

In Sect. 3, we introduce the high-multipole ($\ell \geq 30$) likelihood and present its main results. At these smaller scales, we employ a pseudo-$C_\ell$ approach, beginning with a numerical

---

\* Corresponding author: F. R. Bouchet, bouchet@iap.fr

[1] *Planck* (http://www.esa.int/Planck) is a project of the European Space Agency (ESA) with instruments provided by two scientific consortia funded by ESA member states and led by Principal Investigators from France and Italy, telescope reflectors provided through a collaboration between ESA and a scientific consortium led and funded by Denmark, and additional contributions from NASA (USA).

spherical harmonic transform of the full-sky map, debiased and deconvolved to account for the mask and noise.

Section 4 is devoted to the detailed assessment of this high-$\ell$ likelihood. One technical difference between Like13 and the present work is the move from the `CamSpec` code to `Plik` for high-$\ell$ results as well as the released software (Planck Collaboration ES 2015). The main reason for this change is that the structure of `Plik` allows more fine-grained tests on the polarization spectra for individual detectors or subsets of detectors. We are able to compare the effect of different cuts on *Planck* and external data, as well as using methods that take different approaches to estimate the maximum-likelihood spectra from the input maps; these illustrate the small impact of differences in methodology and data preparation, which are difficult to assess otherwise.

We then combine the low- and high-$\ell$ algorithms to form the full *Planck* likelihood in Sect. 5, assessing there the choice of $\ell = 30$ for the hybridization scale and establishing the basic cosmological results from *Planck* 2015 data alone.

Finally, in Sect. 6 we conclude. A series of Appendices discusses sky masks and gives more detail on the individual likelihood codes, both the released version and a series of other codes used to validate the overall methodology.

To help distinguish the many different likelihood codes, which are functions of different parameters and use different input data, Table 1 summarizes the designations used throughout the text.

## 2. Low-multipole likelihood

At low multipoles, the current *Planck* release implements a standard joint pixel-based likelihood including both temperature and polarization for multipoles $\ell \leq 29$. Throughout this paper, we denote this likelihood "lowTEB", while "lowP" denotes the polarization part of this likelihood. For temperature, the formalism uses the CMB maps cleaned with `Commander` (Eriksen et al. 2004, 2008) maps, while for polarization we use the 70 GHz LFI maps and explicitly marginalize over the 30 GHz and 353 GHz maps taken as tracers of synchrotron and dust emission, respectively (see Sect. 2.3), accounting in both cases for the induced noise covariance in the likelihood.

This approach is somewhat different from the *Planck* 2013 low-$\ell$ likelihood. As described in Like13, this comprised two nearly independent components, covering temperature and polarization information, respectively. The temperature likelihood employed a Blackwell-Rao estimator (Chu et al. 2005) at $\ell \leq 49$, averaging over Monte Carlo samples drawn from the exact power spectrum posterior using `Commander`. For polarization, we had adopted the pixel-based 9-year WMAP polarization likelihood, covering multipoles $\ell \leq 23$ (Bennett et al. 2013).

The main advantage of the exact joint approach now employed is mathematical rigour and consistency to higher $\ell$, while the main disadvantage is a slightly higher computational expense due to the higher pixel resolution required to extend the calculation to $\ell = 29$ in polarization. However, after implementation of the Sherman–Morrison–Woodbury formula to reduce computational costs (see Appendix B.1), the two approaches perform similarly, both with respect to speed and accuracy, and our choice is primarily a matter of implementational convenience and flexibility, rather than actual results or performance.

## 2.1. Statistical description and algorithm

We start by reviewing the general CMB likelihood formalism for the analysis of temperature and polarization at low $\ell$, as described for instance by Tegmark & de Oliveira-Costa (2001), Page et al. (2007a), and in Like13. We begin with maps of the three Stokes parameters $\{T, Q, U\}$ for the observed CMB intensity and linear polarization in some set of `HEALPix`[2] (Górski et al. 2005) pixels on the sky. In order to use multipoles $\ell \leq \ell_{\rm cut} = 29$ in the likelihood, we adopt a `HEALPix` resolution of $N_{\rm side} = 16$ which has 3072 pixels (of area $13.6\,{\rm deg}^2$) per map; this accommodates multipoles up to $\ell_{\rm max} = 3N_{\rm side} - 1 = 47$, and, considering separate maps of $T$, $Q$, and $U$, corresponds to a maximum of $N_{\rm pix} = 3 \times 3072 = 9216$ pixels in any given calculation, not accounting for any masking.

After component separation, the data vector may be modelled as a sum of cosmological CMB signal and instrumental noise, $\boldsymbol{m}^X = \boldsymbol{s}^X + \boldsymbol{n}^X$, where $\boldsymbol{s}$ is assumed to be a set of statistically isotropic and Gaussian-distributed random fields on the sky, indexed by pixel or spherical-harmonic indices $(\ell m)$, with $X = \{T, E, B\}$ selecting the appropriate intensity or polarization component. The signal fields $\boldsymbol{s}^X$ have auto- and cross-power spectra $C_\ell^{XY}$ and a pixel-space covariance matrix

$$\mathsf{S}(C_\ell) = \sum_{\ell=2}^{\ell_{\rm max}} \sum_{XY} C_\ell^{XY} \mathsf{P}_\ell^{XY}. \qquad (1)$$

Here we restrict the spectra to $XY = \{TT, EE, BB, TE\}$, with $N_{\rm side} = 16$ pixelization, and $\mathsf{P}_\ell^{XY}$ is a beam-weighted sum over (associated) Legendre polynomials. For temperature, the explicit expression is

$$(\mathsf{P}_\ell^{TT})_{i,j} = \frac{2\ell + 1}{4\pi} B_\ell^2 P_\ell(\hat{\boldsymbol{n}}_i \cdot \hat{\boldsymbol{n}}_j), \qquad (2)$$

where $\hat{\boldsymbol{n}}_i$ is a unit vector pointing towards pixel $i$, $B_\ell$ is the product of the instrumental beam Legendre transform and the `HEALPix` pixel window, and $P_\ell$ is the Legendre polynomial of order $\ell$; for corresponding polarization components, see, e.g., Tegmark & de Oliveira-Costa (2001). The instrumental noise is also assumed to be Gaussian distributed, with a covariance matrix $\mathsf{N}$ that depends on the *Planck* detector sensitivity and scanning strategy, and the full data covariance is therefore $\mathsf{M} = \mathsf{S} + \mathsf{N}$. With these definitions, the full likelihood expression reads

$$\mathcal{L}(C_\ell) = \mathcal{P}(\boldsymbol{m}|C_\ell) = \frac{1}{2\pi|\mathsf{M}|^{1/2}} \exp\left(-\frac{1}{2}\boldsymbol{m}^{\sf T} \mathsf{M}^{-1} \boldsymbol{m}\right), \qquad (3)$$

where the conditional probability $\mathcal{P}(\boldsymbol{m}|C_\ell)$ defines the likelihood $\mathcal{L}(C_\ell)$.

The computational cost of this expression is driven by the presence of the matrix inverse and determinant operations, both of which scale computationally as $O(N_{\rm pix}^3)$. For this reason, the direct approach is only computationally feasible at large angular scales, where the number of pixels is low. In practice, we only analyse multipoles below or equal to $\ell_{\rm cut} = 29$ with this formalism, requiring maps with $N_{\rm side} = 16$. Multipoles between $\ell_{\rm cut} + 1$ and $\ell_{\rm max}$ are fixed to the best-fit $\Lambda$CDM spectrum when calculating $\mathsf{S}$. This division between varying and fixed multipoles speeds up the evaluation of Eq. (3) through the Sherman–Morrison–Woodbury formula and the related matrix determinant lemma, as described in Appendix B.1. This results in an order-of-magnitude speed-up compared to the brute-force computation.

---

[2] http://healpix.sourceforge.org

**Table 1.** Likelihood codes and datasets. We use these designations throughout the text to refer to specific likelihood codes and implementations that use different input data. A sum of spectra in the description column designates the joint likelihood of these spectra.

| Name | Description |
| --- | --- |
| PlanckTT ......... | Full *Planck* temperature-only $C_\ell^{TT}$ likelihood |
| PlanckTT,TE,EE .... | PlanckTT combined with high-$\ell$ $C_\ell^{TE} + C_\ell^{EE}$ likelihood |
| lowP ............. | Low-$\ell$ polarization $C_\ell^{TE} + C_\ell^{EE} + C_\ell^{BB}$ likelihood |
| lowTEB ......... | Low-$\ell$ temperature-plus-polarization likelihood |
| PlikTT........... | High-$\ell$ $C_\ell^{TT}$-only likelihood |
| PlikEE........... | High-$\ell$ $C_\ell^{EE}$-only likelihood |
| PlikTE........... | High-$\ell$ $C_\ell^{TE}$-only likelihood |
| PlikTT,TE,EE ..... | High-$\ell$ $C_\ell^{TT} + C_\ell^{TE} + C_\ell^{EE}$ likelihood |
| Plik_lite ........ | High-$\ell$ $C_b^{TT} + C_b^{TE} + C_b^{EE}$, foreground-marginalized bandpower likelihood |
| tauprior ......... | Gaussian prior, $\tau = 0.07 \pm 0.02$ |
| highL ............ | ACT+SPT high-$\ell$ likelihood |
| WP ............. | WMAP low-$\ell$ polarization likelihood[a] |

[a] "Low-$\ell$" refers to $\ell < 23$ for WP, but $\ell < 30$ for the *Planck* likelihoods.

## 2.2. Low-$\ell$ temperature map and mask

Next, we consider the various data inputs that are required to evaluate the likelihood in Eq. (3), and we start our discussion with the temperature component. As in 2013, we employ the Commander algorithm for component separation. This is a Bayesian Monte Carlo method that either samples from or maximizes a global posterior defined by some explicit parametric data model and a set of priors. The data model adopted for the *Planck* 2015 analysis is described in detail in Planck Collaboration X (2016), and reads

$$s_\nu(\theta) = g_\nu \sum_{i=1}^{N_{comp}} \mathsf{F}_\nu^i(\beta_i, \Delta_\nu)\, a_i + \sum_{j=1}^{N_{template}} T_\nu^j b_j^\nu, \qquad (4)$$

where $\theta$ denotes the full set of unknown parameters determining the signal at frequency $\nu$. The first sum runs over $N_{comp}$ independent astrophysical components including the CMB itself; $a_i$ is the corresponding amplitude map for each component at some given reference frequency; $\beta_i$ is a general set of spectral parameters for the same component; $g_\nu$ is a multiplicative calibration factor for frequency $\nu$; $\Delta_\nu$ is a linear correction of the bandpass central frequency; and the function $\mathsf{F}_\nu^i(\beta_i, \Delta_\nu)$ gives the frequency dependence for component $i$ (which can vary pixel-by-pixel and is hence most generally an $N_{pix} \times N_{pix}$ matrix). In the second sum, $T_\nu^j$ is one of a set of $N_{template}$ correction template amplitudes, accounting for known effects such as monopole, dipole, or zodiacal light, with template maps $b_j^\nu$.

In 2013, only *Planck* observations between 30 and 353 GHz were employed in the corresponding fit. In the updated analysis, we broaden the frequency range considerably, by including the *Planck* 545 and 857 GHz channels, the 9-year WMAP observations between 23 and 94 GHz (Bennett et al. 2013), and the Haslam et al. (1982) 408 MHz survey. We can then separate the low-frequency foregrounds into separate synchrotron, free-free, and spinning-dust components, as well as to constrain the thermal dust temperature pixel-by-pixel. In addition, in the updated analysis we employ individual detector and detector-set maps rather than co-added frequency maps, and this gives stronger constraints on both line emission (primarily CO) processes and bandpass measurement uncertainties. For a comprehensive discussion of all these results, we refer the interested reader to Planck Collaboration X (2016).

For the purposes of the present paper, the critical output from this process is the maximum-posterior CMB temperature sky map, shown in the top panel of Fig. 1. This map is natively produced at an angular resolution of 1° FWHM, determined by the instrumental beams of the WMAP 23 GHz and 408 MHz frequency channels. In addition, the Commander analysis provides a direct goodness-of-fit measure per pixel in the form of the $\chi^2$ map shown in Planck Collaboration X (2016, figure 22). Thresholding this $\chi^2$ map results in a confidence mask that may be used for likelihood analysis, and the corresponding masked region is indicated in the top panel of Fig. 1 by a gray boundary. Both the map and mask are downgraded from their native HEALPix $N_{side} = 256$ pixel resolution to $N_{side} = 16$ before insertion into the likelihood code, and the map is additionally smoothed to an effective angular resolution of 440′ FWHM.

The middle panel of Fig. 1 shows the difference between the *Planck* 2015 and 2013 Commander maximum-posterior maps, where the gray region now corresponds to the 2013 confidence mask. Overall, there are large-scale differences at the $10 \,\mu$K level at high Galactic latitudes, while at low Galactic latitudes there are a non-negligible number of pixels that saturate the colour scale of $\pm 25 \,\mu$K. These differences are well understood. First, the most striking red and blue large-scale features at high latitudes are dominated by destriping errors in our 2013 analysis, due to bandpass mismatch in a few frequency channels effectively behaving as correlated noise during map making. As discussed in section 3 of Planck Collaboration X (2016) and illustrated in figure 2 therein, the most significant outliers have been removed from the updated 2015 analysis, and, consequently, the pattern is clearly visible from the difference map in Fig. 1. Second, the differences near the Galactic plane and close to the mask boundary are dominated by negative CO residuals near the Fan region, at Galactic coordinates $(l, b) \approx (110°, 20°)$; by negative free-free residuals near the Gum nebula at $(l, b) \approx (260°, 15°)$; and by thermal dust residuals along the plane. Such differences are expected because of the wider frequency coverage and improved foreground model in the new fit. In addition, the updated model also includes the thermal Sunyaev-Zeldovich (SZ) effect near the Coma and Virgo clusters in the northern hemisphere, and this may be seen as a roughly circular patch near the Galactic north pole.

Overall, the additional frequency range provided by the WMAP and 408 MHz observations improves the component

A better view of these effects is seen in the bottom panel of Fig. 48. Here we plot the binned values from the top panel as deviations from the best-fit model. Naturally, the black bins of the likelihood output fit well, since they were derived jointly with the best-fit spectrum, while correcting for foreground residuals. The WMAP-9 points show good agreement, given their errors, with the *Planck* 2015 best fit, and illustrate very tight control of the large-scale residual foregrounds (at the low-$\ell$ range of the figure); beyond $\ell \sim 600$ the WMAP-9 spectrum shows an increasing loss of fidelity. *Planck* raw 70, 100, and 143 GHz spectra show excess power in the lowest $\ell$ bin due to diffuse foreground residuals. The higher-$\ell$ range now shows more clearly the upward drift of power in the raw spectra, growing from 143 GHz to 70 GHz. This is consistent with the well-determined integrated discrete foreground contributions to those spectra. As previously shown in Planck Collaboration XXXI (2014, figure 8), the unresolved discrete foreground power (computed with the same sky masks as used here) can be represented in the bin near $\ell = 800$ as levels of approximately $40\,\mu K^2$ at 70 GHz, $15\,\mu K^2$ at 100 GHz, and $5\,\mu K^2$ at 143 GHz, in good agreement with the present figure.

### 5.7.2. ACT and SPT

*Planck* temperature observations are complemented at finer scales by measurements from the ground-based Atacama Cosmology Telescope (ACT) and South Pole Telescope (SPT). The ACT and SPT high-resolution data help *Planck* in separating the primordial cosmological signal from other Galactic and extragalactic emission, so as not to bias cosmological reconstructions in the damping-tail region of the spectrum. In 2013 we combined *Planck* with ACT (Das et al. 2013) and SPT (Reichardt et al. 2012) data in the multipole range $1000 < \ell < 10\,000$, defining a common foreground model and extracting cosmological parameters from all the data sets. Our updated "highL" temperature data include ACT power spectra at 148 and 218 GHz (Das et al. 2013) with a revised binning (Calabrese et al. 2013) and final beam estimates (Hasselfield et al. 2013), and SPT measurements in the range $2000 < \ell < 13\,000$ from the 2540 deg$^2$ SPT-SZ survey at 95, 150, and 220 GHz (George et al. 2014). However, in this new analysis, given the increased constraining power of the *Planck* full-mission data, we do not use ACT and SPT as primary data sets. Using the same $\ell$ cuts as the 2013 analysis (i.e., ACT data at $1000 < \ell < 10\,000$ and SPT at $\ell > 2000$) we only check for consistency and retain information on the nuisance foreground parameters that are not well constrained by *Planck* alone.

To assess the consistency between these data sets, we extend the *Planck* foreground model up to $\ell = 13\,000$ with additional nuisance parameters for ACT and SPT, as described in Planck Collaboration XIII (2016, section 4). Fixing the cosmological parameters to the best-fit PlanckTT+lowP base-$\Lambda$CDM model and varying the ACT and SPT foreground and calibration parameters, we find a reduced $\chi^2 = 1.004$ (PTE = 0.46), showing very good agreement between *Planck* and the highL data.

As described in Planck Collaboration XIII (2016), we then take a further step and extend the Gibbs technique presented in Dunkley et al. (2013) and Calabrese et al. (2013) (and applied to *Planck* alone in Sect. 5.6) to extract independent CMB-only band-powers from *Planck*, ACT, and SPT. The extracted CMB spectra are reported in Fig. 49. We also show ACT and SPT band-powers at lower multipoles as extracted by Calabrese et al. (2013). This figure shows the state of the art of current CMB observations, with *Planck* covering the low-to-high-multipole
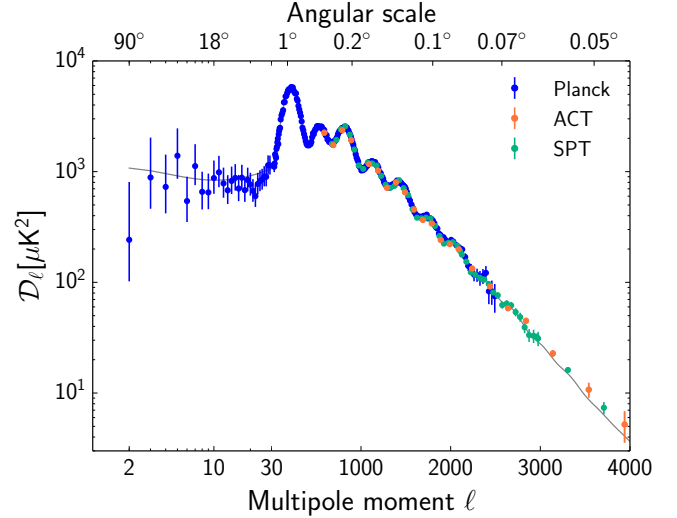


**Figure 49.** CMB-only power spectra measured by *Planck* (blue), ACT (orange), and SPT (green). The best-fit PlanckTT+lowP $\Lambda$CDM model is shown by the grey solid line. ACT data at $\ell > 1000$ and SPT data at $\ell > 2000$ are marginalized CMB band-powers from multi-frequency spectra presented in Das et al. (2013) and George et al. (2014) as extracted in this work. Lower multipole ACT ($500 < \ell < 1000$) and SPT ($650 < \ell < 3000$) CMB power extracted by Calabrese et al. (2013) from multi-frequency spectra presented in Das et al. (2013) and Story et al. (2012) are also shown. The binned values in the range $3000 < \ell < 4000$ appear higher than the unbinned best-fit line because of the binning (this is numerically confirmed by the residual plot in Planck Collaboration XIII 2016, figure 9).

range and ACT and SPT extending into the damping region. We consider the CMB to be negligible at $\ell > 4000$ and note that these ACT and SPT band-powers have an overall calibration uncertainty (2 % for ACT and 1.2 % for SPT).

The inclusion of ACT and SPT improves the full-mission *Planck* spectrum extraction presented in Sect. 5.6 only marginally. The main contribution of ACT and SPT is to constrain small components (e.g., the tSZ, kSZ, and tSZ×CIB) that are not well determined by *Planck* alone. However, those components are sub-dominant for *Planck* and are well described by the prior based on the 2013 *Planck*+highL solutions imposed in the *Planck*-alone analysis. The CIB amplitude estimate improves by 40 % when including ACT and SPT, but the CIB power is also reasonably well constrained by *Planck* alone. The main *Planck* contaminants are the Poisson sources, which are treated as independent and do not benefit from ACT and SPT. As a result, the errors on the extracted *Planck* spectrum are only slightly reduced, with little additional cosmological information added by including ACT and SPT for the baseline $\Lambda$CDM model (see also Planck Collaboration XIII 2016, section 4).

## 6. Conclusions

The *Planck* 2015 angular power spectra of the cosmic microwave background derived in this paper are displayed in Fig. 50. These spectra in $TT$ (top), $TE$ (middle), and $EE$ (bottom) are all quite consistent with the best-fit base-$\Lambda$CDM model obtained from $TT$ data alone (red lines). The horizontal axis is logarithmic at $\ell < 30$, where the spectra are shown for individual multipoles, and linear at $\ell \geq 30$, where the data are binned. The
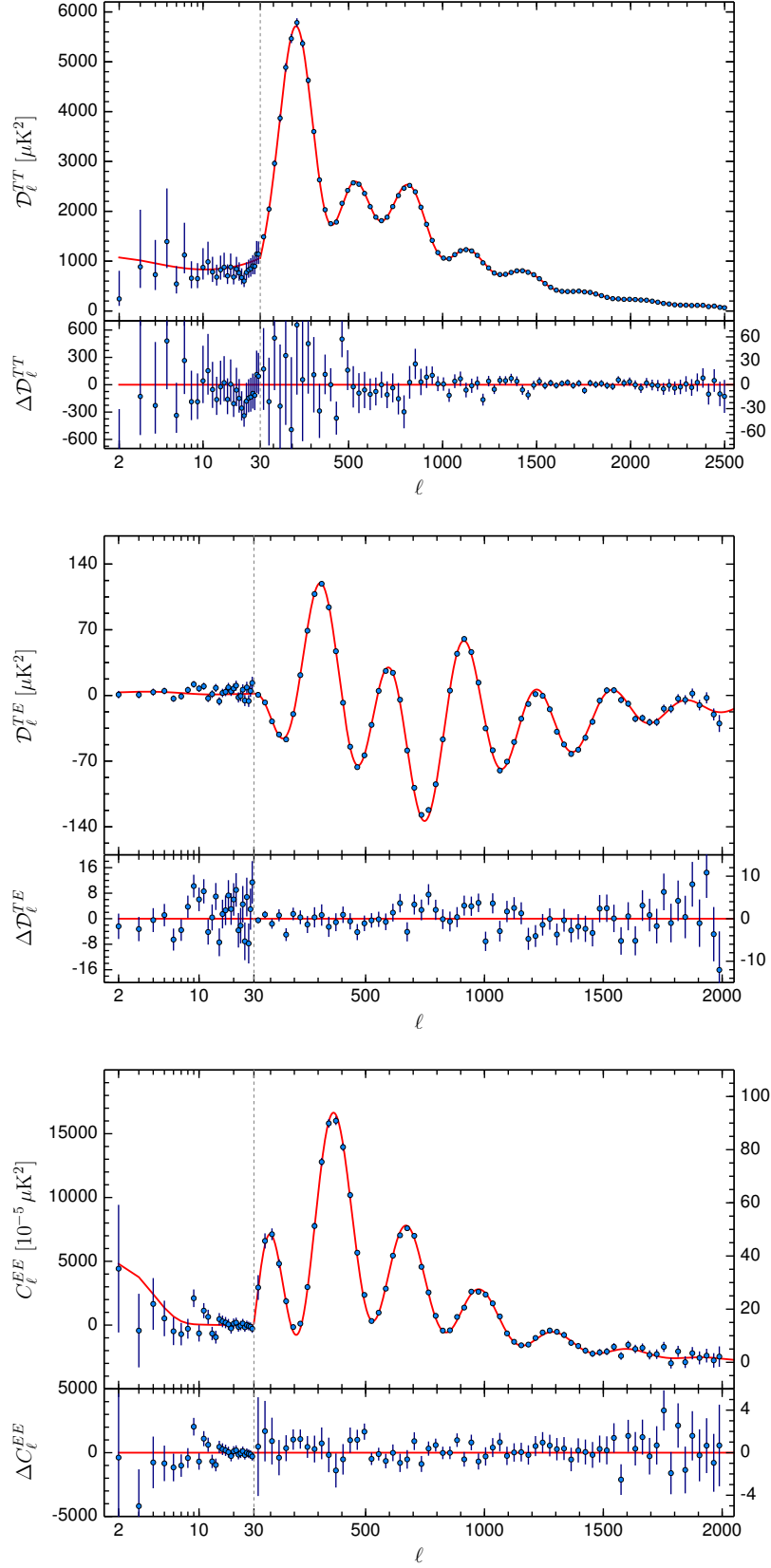
**Figure 50.** *Planck* 2015 CMB spectra, compared with the base ΛCDM fit to PlanckTT+lowP data (red line). The upper panels show the spectra and the lower panels the residuals. In all the panels, the horizontal scale changes from logarithmic to linear at the "hybridization" scale, $\ell = 29$ (the division between the low-$\ell$ and high-$\ell$ likelihoods). For the residuals, the vertical axis scale changes as well, as shown by different left and right axes. We show $\mathcal{D}_\ell = \ell(\ell + 1)C_\ell/(2\pi)$ for $TT$ and $TE$, but $C_\ell$ for $EE$, which also has different vertical scales at low- and high-$\ell$.

error bars correspond to the diagonal elements of the covariance matrix. The lower panels display the residuals, the data being presented with different vertical axes, a larger one at left for the low-$\ell$ part and a zoomed-in axis at right for the high-$\ell$ part.

The 2015 *Planck* likelihood presented in this work is based on more temperature data than in the 2013 release, and on new polarization data. It benefits from several improvements in the processing of the raw data, and in the modelling of astrophysical foregrounds and instrumental noise. Apart from a revision of the overall calibration of the maps, discussed in Planck Collaboration I (2016), the most significant improvements are in the likelihood procedures:

(i) a joint temperature-polarization pixel-based likelihood at $\ell \leq 29$, with more high-frequency information used for foreground removal, and smaller sky masks (Sects. 2.1 and 2.2);

(ii) an improved Gaussian likelihood at $\ell \geq 30$ that includes a different strategy for estimating power spectra from data-subset cross-correlations, using half-mission data instead of detector sets (which enables us to reduce the effect of correlated noise between detectors, see Sects. 3.2.1 and 3.4.3), and better foreground templates, especially for Galactic dust (Sect. 3.3.1) that lets us mask a smaller fraction of the sky (Sect. 3.2.2) and to retain large-angle temperature information from the 217 GHz map that was neglected in the 2013 release (Sect. 3.2.4).

We performed several consistency checks of the robustness of our likelihood-making process, by introducing more or less freedom and nuisance parameters in the modelling of foregrounds and instrumental noise, and by including different assumptions about the relative calibration uncertainties across frequency channels and about the beam window functions.

For temperature, the reconstructed CMB spectrum and error bars are remarkably insensitive to all these different assumptions. Our final high-$\ell$ temperature likelihood, referred to as "PlanckTT" marginalizes over 15 nuisance parameters (12 modelling the foregrounds, and 3 for calibration uncertainties). Additional nuisance parameters (in particular, those associated with beam uncertainties) were found to have a negligible impact, and can be kept fixed in the baseline likelihood. Detailed end-to-end simulations of the instrumental response to the sky analysed like the real data did not uncover hidden low-level residual systematics.

For polarization, the situation is different. Variation of the assumptions leads to scattered results, with greater deviations than would be expected due to changes in the data subsets used, and at a level that is significant compared to the statistical error bars. This suggests that further systematic effects need to be either modelled or removed. In particular, our attempt to model calibration errors and temperature-to-polarization leakage suggests that the $TE$ and $EE$ power spectra are affected by systematics at a level of roughly $1\,\mu\mathrm{K}^2$. Removal of polarization systematics at this level of precision requires further work, beyond the scope of this release. The 2015 high-$\ell$ polarized likelihoods, referred to as "PlikTE" and "PlikEE", or "PlikTT,EE,TE" for the combined version, ignore these uncertain corrections. They only include 12 additional nuisance parameters accounting for polarized foregrounds. Although these likelihoods are distributed in the *Planck* Legacy Archive,[18] we stick to the PlanckTT+lowP choice in the baseline analysis of this paper and the companion papers such

as Planck Collaboration XIII (2016), Planck Collaboration XIV (2016), and Planck Collaboration XX (2016).

We developed internally several likelihood codes, exploring not only different assumptions about foregrounds and instrumental noise, but also different algorithms for building an approximate Gaussian high-$\ell$ likelihood (Sect. 4.2). We compared these codes to check the robustness of the results, and decided to release:

(i) A baseline likelihood called Plik (available for $TT$, $TE$, $EE$, or combined observables), in which the data are binned in multipole space, with a bin-width increasing from $\Delta\ell = 5$ at $\ell \approx 30$ to $\Delta\ell = 33$ at $\ell \approx 2500$.

(ii) An unbinned version which, although slower, is preferable when investigating models with sharp features in the power spectra.

(iii) A simplified likelihood called Plik_lite in which the foreground templates and calibration errors are marginalized over, producing a marginalized spectrum and covariance matrix. This likelihood does not allow investigation of correlations between cosmological and foreground/instrumental parameters, but speeds up parameter extraction, having no nuisance parameters to marginalize over.

In this paper we have also presented an investigation of the measurement of cosmological parameters in the minimal six-parameter $\Lambda$CDM model and a few simple seven-parameter extensions, using both the new baseline *Planck* likelihood and several alternative likelihoods relying on different assumptions. The cosmological analysis of this paper does not replace the investigation of many extended cosmological models presented, e.g., in Planck Collaboration XIII (2016), Planck Collaboration XIV (2016), and Planck Collaboration XX (2016). However, the careful inspection of residuals presented here addresses two questions:

(i) a priori, is there any indication that an alternative model to $\Lambda$CDM could provide a significantly better fit?

(ii) if there is such an indication, could it come from caveats in the likelihood-building (imperfect data reduction, foreground templates or noise modelling) instead of new cosmological ingredients?

Since this work is entirely focused on the power-spectrum likelihood, it can only address these questions at the level of 2-point statistics; for a discussion of higher-order statistics, see Planck Collaboration XVI (2016) and Planck Collaboration XVII (2016).

The most striking result of this work is the impressive consistency of different cosmological parameter extractions, performed with different versions of the PlikTT+tauprior or PlanckTT+lowP likelihoods, with several assumptions concerning: data processing (half-mission versus detector set correlations); sky masks and foreground templates; beam window functions; the use of two frequency channels instead of three; different cuts at low $\ell$ or high $\ell$; a different choice for the multipole value at which we switch from the pixel-based to the Gaussian likelihood; different codes and algorithms; the inclusion of external data sets like WMAP-9, ACT, or SPT; and the use of foreground-cleaned maps (instead of fitting the CMB+foreground map with a sum of different contributions). In all these cases, the best-fit parameter values drift by only a small amount, compatible with what one would expect on a statistical basis when some of the data are removed (with a few exceptions summarized below).

---

The cosmological results are stable when one uses the simplified `Plik_lite` likelihood. We checked this by comparing PlanckTT+lowP results from `Plik` and `Plik_lite` for ΛCDM, and for six examples of seven-parameter extended models.

Another striking result is that, despite evidence for small unsolved systematic effects in the high-$\ell$ polarization data, the cosmological parameters returned by the `PlikTT`, `PlikTE`, or `PlikEE` likelihoods (in combination with a $\tau$ prior or *Planck* lowP) are consistent with each other, and the residuals of the (frequency combined) $TE$ and $EE$ spectra after subtracting the temperature ΛCDM best-fit are consistent with zero. As has been emphasized in other *Planck* 2015 papers, this is a tremendous success for cosmology, and an additional proof of the predictive power of the standard cosmological model. It also suggests that the level of temperature-to-polarization leakage (and possibly other systematic effects) revealed by our consistency checks is low enough  (on average over all frequencies) not to significantly bias parameter extraction, at least for the minimal cosmological model. We do not know yet whether this conclusion applies also to extended models, especially those in which the combination of temperature and polarization data has stronger constraining power than temperature data alone, e.g., dark matter annihilation (Planck Collaboration XIII 2016) or isocurvature modes (Planck Collaboration XX 2016). One should thus wait for a future *Planck* release before applying the *Planck* temperature-plus-polarization likelihood to such models. However, the fact that we observe a significant reduction in the error bars when including polarization data is very promising, since this reduction is expected to remain after the removal of systematic effects.

Careful inspection of residuals with respect to the best-fit ΛCDM model has revealed a list of anomalies in the *Planck* CMB power spectra, of which the most significant is still the low-$\ell$ temperature anomaly in the range $20 \le \ell \le 30$, already discussed at length in the 2013 release. In this 2015 release, with more data and with better calibration, foreground modelling, and sky masks, its significance has decreased from the 0.7 % to the 2.8 % level for the $TT$ spectrum (Sect. 5.5). This probability is still small (although not very small), and the feature remains unexplained. We have also investigated the $EE$ spectrum, where the anomaly, if any, is significant only at the 7.7 % level.

Other "anomalies" revealed by inspection of residuals (and of their dependence on the assumptions underlying the likelihood) are much less significant. There are a few bins in which the power in the $TT$, $TE$, or $EE$ spectrum lies 2–3 $\sigma$ away from the best-fit ΛCDM prediction, but this is not statistically unlikely and we find acceptable probability-to-exceed (PTE) levels. Nevertheless, in Sects. 3.8 and 4.1, we presented a careful investigation of these features, to see whether they could be caused by some imperfect modelling of the data. We noted that a deviation in the $TT$ spectrum at $\ell \approx 1450$ is somewhat suspicious, since it is driven mostly by a single channel (217 GHz), and since it depends on the foreground-removal method. But this deviation is too small to be worrisome (1.8 $\sigma$ with the baseline `Plik` likelihood). As in the 2013 release, the data at intermediate $\ell$ would be fitted slightly better by a model with more lensing than in the best-fit ΛCDM model (to reduce the peak-to-trough contrast), but more lensing generically requires higher values of $A_s$ and $\Omega_c h^2$ that are disfavoured by the rest of the data, in particular when high-$\ell$ information is included. This mild tension is illustrated by the preference for a value greater than unity for the unphysical parameter $A_L$, a conclusion that is stable against variations in the assumptions underlying the likelihoods. However, $A_L$ is compatible with unity at the 1.8 $\sigma$ level when using the baseline PlanckTT likelihood with a conservative $\tau$ prior (to

avoid the effect of the low-$\ell$ dip), so what we see here could be the result of statistical fluctuations.

This absence of large residuals in the *Planck* 2015 temperature and polarization spectra further establishes the robustness of the ΛCDM model, even with about twice as much data as in the *Planck* 2013 release. This conclusion is supported by several companion papers, in which many non-minimal cosmological models are investigated but no significant evidence for extra physical ingredients is found. The ability of the temperature results to pass several demanding consistency tests, and the evidence of excellent agreement down to the $\mu K^2$ level between the temperature and polarization data, represent an important milestone set by the *Planck* satellite. The *Planck* 2015 likelihoods are the best illustration to date of the predictive power of the minimal cosmological model, and, at the same time, the best tool for constraining interesting, physically-motivated deviations from that model.

# References

Aad, G. e. a., Measurement of the Higgs boson mass from the $H \to \gamma\gamma$ and $H \to ZZ^* \to 4\ell$ channels in $pp$ collisions at center-of-mass energies of 7 and 8 TeV with the ATLAS detector. 2014, Phys. Rev. D, 90, 052004 E.5

Addison, G. E., Dunkley, J., & Spergel, D. N., Modelling the correlation between the thermal Sunyaev Zel'dovich effect and the cosmic infrared background. 2012, MNRAS, 427, 1741, arXiv:1204.5927 3.3.2

Addison, G. E., Huang, Y., Watts, D. J., et al., Quantifying discordance in the 2015 Planck CMB spectrum. 2015, arXiv:1511.00055 4.1.6, 14, C.5

Arnaud, M., Pratt, G. W., Piffaretti, R., et al., The universal galaxy cluster pressure profile from a representative sample of nearby systems (REXCESS) and the $Y_{SZ}$ - $M_{500}$ relation. 2010, A&A, 517, A92, arXiv:0910.1234 D.2

Audren, B., Lesgourgues, J., Benabed, K., & Prunet, S., Conservative constraints on early cosmology with MONTE PYTHON. 2013, J. Cosmology Astropart. Phys., 2, 1, arXiv:1210.7183 6

Battaglia, N., Natarajan, A., Trac, H., Cen, R., & Loeb, A., Reionization on Large Scales. III. Predictions for Low-l Cosmic Microwave Background Polarization and High-l Kinetic Sunyaev-Zel'dovich Observables. 2013, ApJ, 776, 83, arXiv:1211.2832 D.2

Bennett, C. L., Larson, D., Weiland, J. L., et al., Nine-year Wilkinson Microwave Anisotropy Probe (WMAP) Observations: Final Maps and Results. 2013, ApJS, 208, 20, arXiv:1212.5225 1, 2, 2.2, 2, 2.6

Benoît, A., Ade, P., Amblard, A., et al., Cosmological constraints from Archeops. 2003, A&A, 399, L25, arXiv:astro-ph/0210306 E.2

Béthermin, M., Daddi, E., Magdis, G., et al., A Unified Empirical Model for Infrared Galaxy Counts Based on the Observed Physical Evolution of Distant Galaxies. 2012, ApJ, 757, L23, arXiv:1208.6512 4.3

Béthermin, M., Wang, L., Doré, O., et al., The redshift evolution of the distribution of star formation among dark matter halos as seen in the infrared. 2013, A&A, 557, A66, arXiv:1304.3936 4.3

Blas, D., Lesgourgues, J., & Tram, T., The Cosmic Linear Anisotropy Solving System (CLASS). Part II: Approximation schemes. 2011, JCAP, 07, 034 D.2

Bond, J. R., Contaldi, C., & Pogosyan, D., Cosmic microwave background snapshots: pre-WMAP and post-WMAP. 2003, Royal Society of London Philosophical Transactions Series A, 361, 2435, arXiv:astro-ph/0310735 E.2